PHYSICAL REVIEW B VOLUME 33, NUMBER 3 1 FEBRUARY 1986

Molecular-dynamics study of surface premelting effects

V. Rosato

Section de Recherches de Métallurgie Physique, Centre d'Etudes Nucléaires de Saclay, 91191 Gif-sur-Yvette Cedex, France

G. Ciccotti

Dipartimento di Fisica Guglielmo Marconi, Università degli Studi "La Sapienza," piazzale Aldo Moro 2, I-00185 Roma, Italy

V. Pontikis*

Section de Recherches de Métallurgie Physique, Centre d'Etudes Nucléaires de Saclay, 91191 Gif-sur-Yvette Cedex, France

(Received 1 July 1985)

The thermodynamical and structural behavior of a (110) face of a fcc (12-6) Lennard-Jones solid has been investigated by molecular-dynamics simulation on the solid-gas coexistence line. The temperature dependence of the relevant structural and mass-transport properties shows the following. (a) Despite the high degree of disorder which gradually appears on surface layers when the temperature is increased, the surface retains its solidlike character up to temperatures ($T \approx 0.64\varepsilon/k_B$) very close to the triple point ($T_t = 0.68\varepsilon/k_B$). This conclusion does not confirm the findings of previous theoretical work predicting the formation of a liquid surface layer well below the bulk melting point. (b) The large concentration of vacancy-adatom pairs, produced at the surface in the high-temperature range, accounts for the high values of the surface diffusivity. (c) The Arrhenius plot of defect concentration indicates a progressive decrease of their formation energy for temperatures ranging from $T_r = 0.8T_m$ to the melting point. Consistently, the order parameter decreases slowly with increasing temperature up to T_r but from $T = T_r$ to the melting point it decreases much more rapidly than predicted by the extrapolation of the low-temperature data. These results are qualitatively consistent with the onset of a surface-roughening transition, in agreement with recent experimental results obtained from helium scattering on (110) copper surfaces.

I. INTRODUCTION

The melting of solids has been the object of intensive investigations from both the theoretical and the experimental points of view. Due to the absence of observable superheating effects on most materials, and particularly on metals, the assumption has been made that melting is a surface-initiated process or, more generally, an interface-initiated process.

According to that assumption, premelting effects which are absent in the bulk[1] can be expected on free surfaces or interfaces, thus propagating melting into the bulk. Theoretical arguments, based on simplified analytical models,[2-4] or computer simulations,[5-7] agree about the surface instability at temperatures lower than the melting point. However, some additional work is still needed to identify clearly the nature of this instability.

The surface-initiated melting can be driven either by a structural instability of the surface, related to anharmonic effects and the enhanced production of defects, or by the formation of a surface liquid layer.

There has been a certain tendency to identify surface premelting effects with the formation of a liquid layer on the surface before melting.[1] The formation of a liquid layer can be thermodynamically justified by considering the interfacial free energies for the solid in equilibrium with its own liquid and vapor phases:[8]

$$\Gamma_{sv} + \delta\Gamma = \Gamma_{sl} + \Gamma_{lv} ,$$

where Γ_{ab} is the free energy of the ab interface (s, l, and v, respectively, denote solid, liquid, and vapor) and $\delta\Gamma \rightarrow 0$ when the temperature reaches the melting-point value.

The sign of $\delta\Gamma$ determines the possible existence of a liquid thin film on the solid surface for temperatures lower than the bulk melting point.

The widespread opinion supporting this macroscopic description of premelting phenomena[2-5], has been recently weakened by the work of Broughton and Gilmer,[6(a)-6(c)] who have interpreted the surface instability in terms of surface roughening.

On the experimental side, the earliest information concerning the structure of surfaces in the high-temperature range ($T > 0.5T_m$) was provided by surface-diffusion studies. Gjostein[9] gave the first evidence of an upward curvature in the Arrhenius plot of the diffusion coefficient of both fcc and bcc metals for temperatures higher than $T = 0.7T_m$. This has been confirmed by a more recent compilation of surface experimental diffusion data by Bonzel.[10] The Arrhenius-plot curvature has been interpreted either as a melting of surface layers[11] or as a consequence of a surface roughening[12] and the subsequent activation of new diffusion mechanisms when temperature increases. The reason for these opposite points of view can be ascribed to the fact that diffusion properties alone are a rather poor tool with which to resolve the atomic structure of surfaces.

More recently, Fritsch *et al.*[13(a),13(b)] measured the specific heat of very thin disks of gallium in a temperature range $T=1.5$ K just below the melting point. The geometry of their samples was chosen in such a way that they could study the contribution of the surface to the specific heat. They observed a sharp increase of the specific heat starting just before the melting temperature ($T=T_m-0.2$ K). Their interpretation is that surface melting occurs in that temperature range. We stress, however, that without an analysis of the surface structure, such a conclusion cannot be justified. In any event, their results are consistent with a structural instability of the surface occurring in the given range of temperature.

A complementary indication of the existence of surface instabilities comes from recent work by Lapujoulade *et al.*[14] They studied the structure of high-index surfaces of copper as a function of temperature by helium scattering and found strong evidence for a surface roughening starting from temperatures as low as $T=0.3T_m$. Due to the difficulties of deconvoluting the diffracted beam intensities, the atomic positions on the surface could not be obtained unambiguously. Nevertheless Villain *et al.*,[15] starting from an atomistic model of step roughness, were able to give an interpretation of the decrease of the diffracted beam intensities consistent with the results of Lapujoulade *et al.*[14]

These results support the idea that the structural instability of the surface is rather a kind of roughening transition than a melting of surface layers.

Grain boundaries, considered as phase boundaries, are analogous to surfaces for many properties such as mass transport and, presumably, premelting effects. A first result was obtained by Kikuchi and Cahn,[16] predicting the occurrence of a premelting transition for a lattice-gas model of a grain boundary. More recently, Ciccotti *et al.*[17] showed that, with increasing temperature, high-angle grain boundaries evolve toward a highly disordered structure which remains, nevertheless, solidlike up to the bulk melting temperature.

In the present work we proceed, as in Ref. 17, to investigate the temperature dependence of surface structure. We find no evidence for surface melting, at least up to the highest investigated temperature: $T=0.643$ versus $T_m=0.68$ (temperature is given in reduced units of ε/k_B), whereas for the special surface we choose, namely the (110) fcc face, melting has been predicted to occur as early as $T=0.5T_m$.[5]

Our results show that on surface layers a structural transition occurs, monitored by the high rate of production of point defects. This transition cannot be classified as a solid-liquid transition, in agreement with the findings of Goodman and Somorjai,[18] but is rather connected to a surface roughening.

These authors used the low-energy electron-diffraction (LEED) technique to study bismuth and tin single-crystal surfaces. They found that the surface structure remains unchanged and that long-range order is maintained up to the respective bulk melting temperatures for these materials and for all the crystal faces investigated. Moreover, we show that an overly large surface-to-volume energy ratio can lead to bulk-driven premelting effects for the simulated model at temperatures well below the argon bulk melting point. Similar effects have been reported by Briant and Burton for argon microclusters.[19]

Previous studies by Broughton and Woodcock[5] and Broughton and Gilmer[6(b)] may have underestimated this fact because their choice of surface-to-volume ratio is unfavorable.

In Sec. II we describe the computational model and related details; in Sec. III we present the results we obtained, while Sec. IV is devoted to some concluding remarks.

II. MODEL AND COMPUTATIONS

A. Model

The model used for the computations consists of an assembly of N point particles arranged on a fcc lattice. We used systems of different sizes, namely $N=673$, 1345, and 2688. A box in the shape of a parallelepiped has been used, with the X, Y, and Z directions along the $[\bar{1}10]$, [001], and [110] crystallographic axes, respectively. This choice defines along the Z direction a repetition of (110) planes in the well-known fcc-structure twofold stacking sequence ($ABAB\cdots$) with a periodicity of $a/\sqrt{2}$, where a is the lattice parameter [Fig. 1(a)].

The models of different sizes have an identical XY section, so that the areas of the (110) planes and the number N_1 of particles belonging to each atomic plane are constant. The procedure generates systems with a number of (110) atomic planes, $N_p=14$, 28, and 56, respectively, for the three values of N given above (Table I).

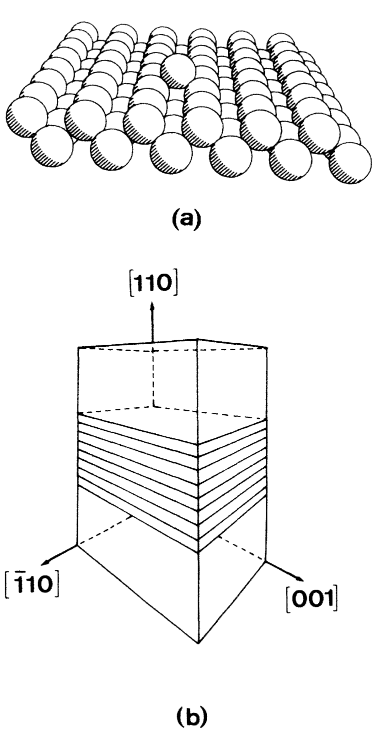

FIG. 1. (a) Geometrical arrangement of the first two layers of our models, parallel to a (110) fcc surface. An adatom is shown located on an equilibrium site. (b) Schematic view of the computational box partially filled with the crystal.

TABLE I. Geometrical characteristics of the different systems used in this work. N is the total number of particles, N_p the number of (110) atomic planes parallel to the free surfaces, and N_1 the number of particles contained in each atomic plane.

N	N_p	N_1	Periodicity	Remarks
673	14	48	6[001]×8[$\bar{1}$10]×16[110]	one adatom
1345	28	48	6[001]×8[$\bar{1}$10]×28[110]	one adatom
2688	56	48	6[001]×8[$\bar{1}$10]×56[110]	

Along the [$\bar{1}$10] and [001] directions we imposed the ordinary periodic boundary conditions. On the other hand, along the [110] direction the periodicity is defined for a box length larger than the dimension of the lattice along that direction [see Fig. 1(b)]. The empty parts of the box left at the top and at the bottom of the crystal can be filled by particles promoted to the vapor phase. Periodic boundary conditions for the [110] direction guarantee the conservation of N, because a particle escaping from the top (bottom) is reinserted at the bottom (top).

In all the models the free surfaces are not allowed to interact directly or with their respective images, their relative distances through the bulk or the vapor phase being fixed at values larger than the cutoff radius for interactions. The particles interact via the well-known Lennard-Jones central-force, pairwise-additive potential: $V(r)=4\varepsilon[(\sigma/r)^{12}-(\sigma/r)^{6}]$.

Reduced units are used throughout this work, σ for length, ε for energy, and $\tau=(m\sigma^2/\varepsilon)^{1/2}$ for time ($\sigma=3.405$ Å, $\varepsilon=119.8$ K, and $\tau\sim 2.156\times10^{-12}$ s for argon).

The Newtonian equations of motion are integrated by the usual central-difference algorithm with a time step $h=0.0046$.[20] Contributions to atomic forces were considered within a spherical cutoff radius $r_c=3.17$, i.e., between the sixth and seventh neighbors. The values of the thermodynamical quantities have been corrected, when necessary, with the standard long-range terms. The calculated correction takes into account the presence of free surfaces, as shown in the Appendix.

At each temperature the lattice parameter of the model was fitted to the experimental value for solid argon in equilibrium with the vapor phase, according to a compilation of various experimental results due to Pollack.[21]

B. Computations

To obtain equilibrium at a given temperature, the system was allowed to evolve during 2000 time steps. Temperature, potential, and total energy of the system were satisfactorily stable after this initial equilibration run, but the density profiles along the normal to the free surfaces showed that equilibrium was not reached, especially in the high-temperature range. Figures 2(a) and 2(b) represent such density profiles obtained from averages over 100 and 2000 time steps, respectively.

The spurious aspect of the density profile in Fig. 2(b) was the result of periodic oscillations of the interlayer spacing along the direction normal to free surfaces.

These oscillations occurred with a period of a few hundred time steps, thus explaining the differences between short- [Fig. 2(a)] and long-time [Fig. 2(b)] density averages.

This phenomenon is induced by the undamped collective motion of atomic layers parallel to free surfaces and is related to a nonzero value of their net translational velocity although the total translational velocity of the model is zero. To avoid this undesirable effect, the following procedure was used for all the runs during the first 2000 time steps: For each atomic layer parallel to the free surfaces and each time step, we calculated the scalar product $s_i=\bar{f}_i\bar{v}_i$, where $\bar{f}_i$ and $\bar{v}_i$ are the total force and the to-

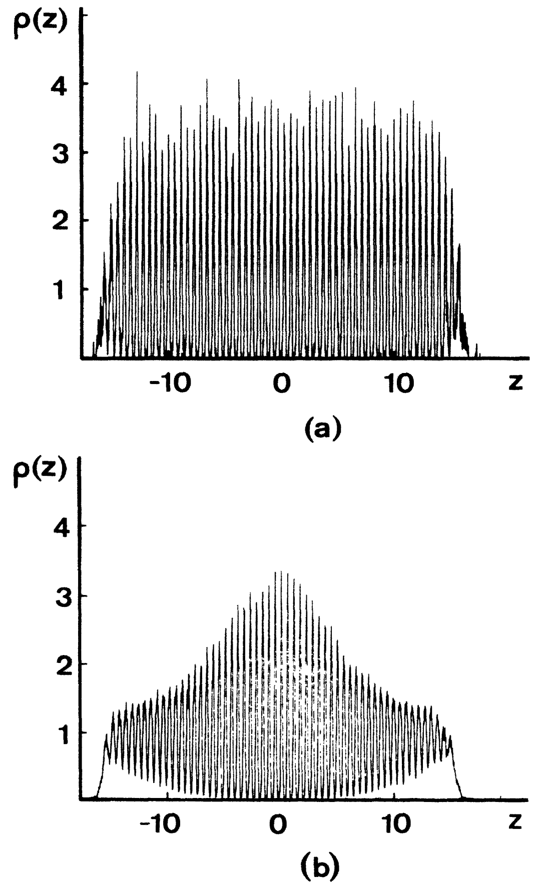

FIG. 2. Density profiles in arbitrary units along a [110] direction (normal to free surfaces) at $T=0.556$ for the $N=2688$ particles system. (a) Average over 100 times steps. (b) Average over 2000 time steps.

TABLE II. List of thermodynamical results; N is the number of particles, T the temperature, ρ the density, U/N the potential energy per particle, and $\beta P/\rho$ the compressibility factor, both including the long-range corrections, evaluated as in the Appendix.

N	T (ε/k_B)	ρ	U/N (ε)	$\beta P/\rho$
673	0.330	1.033	−7.316	−1.327
673	0.465	1.008	−6.937	−0.905
673	0.583	0.984	−6.492	−0.695
1345	0.617	0.971	−6.826	−0.663
2688	0.358	1.032	−7.820	−1.024
2688	0.556	0.984	−7.327	−0.812
2688	0.614	0.975	−7.147	−0.629
2688	0.643	0.969	−7.054	−0.551
1344[a]	0.000	1.054	−8.602	−0.837
1344[a]	0.342	1.032	−8.046	−0.780
1344[a]	0.688	0.967	−7.317	0.187

[a] Perfect crystal.

tal velocity for layer i. If $s<0$, a new set of velocities was assigned to the particles in that layer, sampled from a Maxwellian distribution at the given temperature and satisfying the condition of having a zero value for the translational velocity $\bar{v}_i$. For positive s_i values the layer dynamics was not modified.

This procedure gave satisfactory equilibrium properties and required 2000 time steps. An additional unperturbed trajectory of 2000 time steps was generated for each system; this concluded the equilibration procedure. These first 4000 time steps were excluded from the calculation of thermodynamical averages.

We studied, at the solid-vapor coexistence density, the three systems presented above at temperatures ranging from $T=0.33$ to $T=0.643$. Moreover, for reference purposes, we simulated a perfect solid at various temperatures and densities defined on the solid-vapor coexistence line of the argon phase diagram.

The typical equilibrium computation lasted 4100 time steps (41 ps). Each time step required $\sim$4.9 s of CPU (central processing unit) time on a Hitachi, Inc. NAS9080 computer for the largest system we used. A number of thermodynamical results are collected in Table II.

C. Model reliability

It is necessary that the bulk in our model reproduces the behavior of an infinite solid at the same temperature. Figure 3(a) demonstrates that this requirement is not met for the system of $N=673$ particles at $T=0.583$. The perturbation due to the free surfaces propagates into the bulk and reduces to a few atomic planes the region for which the interlayer spacing is equal to that of an infinite solid. By increasing the thickness of the model up to $N_p=56$ atomic layers [Fig. 3(b)], the bulk interlayer spacing along the normal to free surfaces reaches a value which is close to that of the infinite solid for the largest part of the system, even at the highest temperature we investigated, $T=0.643$. It is for this reason that we use such a thick model.

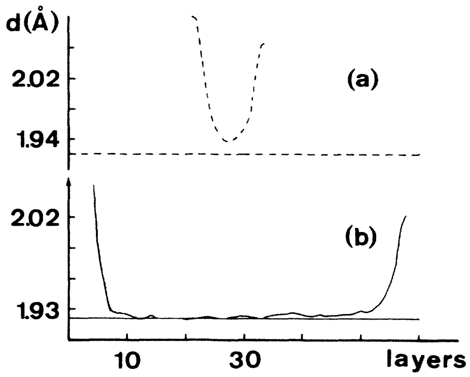

FIG. 3. Interlayer-spacing profile used as a reliability parameter for the different models we used. (a) $N=673$, $T=0.583$. (b) $N=2688$, $T=0.556$. The horizontal lines indicate the lattice parameter of the infinite solid at the given temperatures.

Near the free surfaces, outward relaxation is observed [Figs. 3(a) and 3(b)]. Lennard-Jones potentials lead systematically to outward relaxation of surface layers, as do other empirical pair potentials.[22] Whether such a relaxation is realistic or not cannot be checked in absence of experimental results for solid argon.

The surface-to-volume ratio S/V is another important parameter which determines the thermodynamical behavior of our models with respect to the phase diagram. Figure 4 represents the $E=E(T)$ experimental phase diagram for argon,[23] where E is the total energy per particle. We report the thermodynamical data calculated for our different models and the results of previous simulation work on fcc solid argon obtained by Hansen and Klein[24]

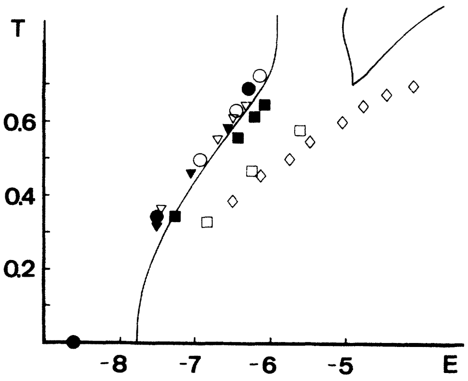

FIG. 4. Experimental argon phase diagram (solid line): $E=E(T)$ (Ref. 23). E is the total energy per particle and T the temperature. Solid circles, periodic solid ($N=1344$); open circles, periodic solid data from Ref. 24; solid squares, free surfaces ($N=2688$); open squares, free surfaces ($N=673$); open triangles, free surfaces ($N=2688$), data for bulk layers; solid triangles, free surfaces ($N=673$), data for bulk layers; open diamonds, free-surface data from Ref. 5. The MD data of the present study contain the long-range correction.

and Broughton and Woodcock.[5] Moreover, for reference purposes we report on this diagram the thermodynamical points calculated for an infinite perfect solid of $N=1344$ particles.

This figure clearly shows that only the largest of our models reproduces thermodynamical data in satisfactory agreement with the infinite-solid data and experiment. For small-size systems, $N=673$, and large S/V values, the thermodynamical data lie well inside the solid-vapor coexistence domain and justify the occurrence of bulk-driven surface premelting effects, similar to those obtained by Broughton and Woodcock.[5]

Therefore we used small systems only for preliminary work and at low temperatures, as the main structural data close to the triple point were obtained principally from the largest system ($N=2688$).

The thermodynamic properties of our systems were also investigated locally. For this purpose we computed on a local basis, that is, for each atomic layer parallel to the surface, the smoothed values of local density, potential energy, pressure, defect concentration, and the Kth component, $\overline{K}=(0,2\pi/a,0)$, of the Fourier transform of the density. In addition, for surface layers we computed the velocity autocorrelation functions and their time integrals (Kubo formulas) to determine the surface self-diffusion coefficients. The computation of these quantities has been detailed elsewhere.[17]

III. RESULTS

A. Local equilibrium properties

Near the free surfaces the local values of potential energy, pressure, and density are significantly different from those obtained in the bulk. These values, corrected to include the long-tail contributions to the pressure and potential energy as indicated in the Appendix, are given in Table III for the different temperatures we studied.

Figure 5 shows a typical density profile averaged over 4100 equilibrium steps at $T=0.643$ for the system of $N=2688$ particles. The production of vacancy-adatom pairs results in the creation of extra layers of adatoms whose positions are shown by the arrows on this figure. In addition, partial overlap of surface layers occurs because of (i) large vibrational amplitudes of atoms on surfaces as compared to those in the bulk, and (ii) very active diffusion processes operating near the melting point.

The potential energy per atom rises from bulk layer values, similar to those obtained for an infinite solid, to values for surface layers which are much larger (Table III). The values of the energy for the bulk layers do not provide, however, a sufficient criterion to guarantee the thermodynamical stability of our systems, as has been discussed above (Sec. II B).

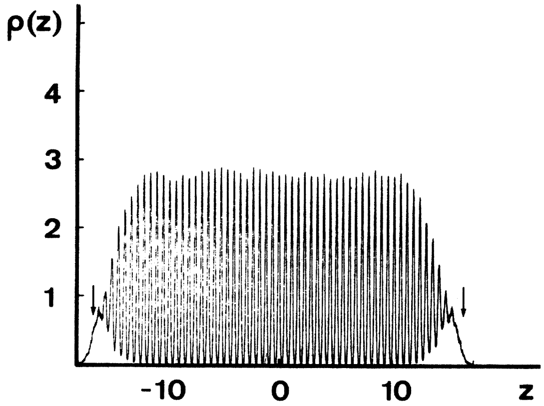

FIG. 5. Equilibrium density profile along the [110] direction, normal to the free surfaces: average over 4100 time steps, $N=2688$, $T=0.643$. Arbitrary units are used for density. Arrows indicate the position of adatom extra layers.

The pressure profiles obtained for the $N=2688$ particle system for the different temperatures we studied are displayed in Fig. 6. The bulk of the crystal is in depression, as indicated by the small negative values of the "plateau" region. This behavior is related to the fact that the crystal dimensions parallel to the free surfaces, fixed at a value depending on the experimental lattice parameter, are kept at this value by the periodic boundary conditions. This value certainly differs from the equilibrium one adapted to the Lennard-Jones potential at a given temperature. Nonetheless, the difference is obviously very small, because the values of the pressure in the bulk are of the order of magnitude of the error made in evaluating this quantity on the solid-vapor coexistence line. Near the free surfaces the pressure values depart from the uniform bulk value, but no simple relationship connects them to the local density and temperature with respect to the phase diagram.

Since steps or other defects are absent from our perfect (110) surfaces, point defects at thermodynamical equilibrium are generated by adatom-vacancy pairs. The averaged concentration of vacancies (adatoms) has been evaluated for the first two atomic layers at the different temperatures we studied; these results are shown in the Arrhenius plots in Fig. 7.

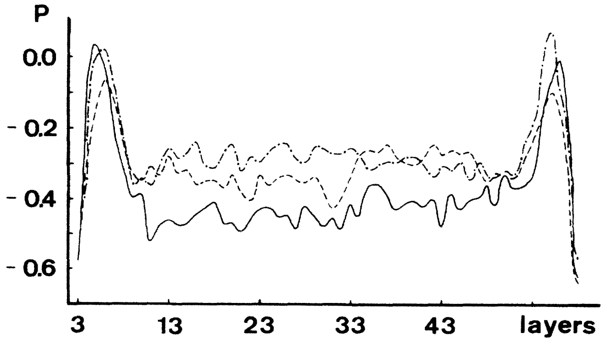

FIG. 6. Equilibrium pressure profiles, $N=2688$. (a) Solid line, $T=0.556$; (b) dashed line, $T=0.614$; (c) dotted-dashed line, $T=0.643$. The long-tail correction (see Appendix) has been included.

The creation of point defects is a thermally activated

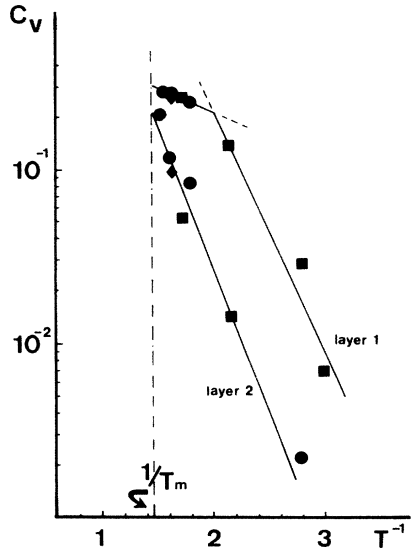

FIG. 7. Arrhenius plots of the vacancy concentration for the two first layers of our systems. Solid circles, $N=2688$, solid diamonds, $N=1345$; solid squares, $N=673$.

process whose activation energy is given by the slope of the linear least-squares fit of the vacancy-concentration data. One can see from Fig. 7 that the data obtained for the first surface layer cannot be fitted by a single straight line.

The activation energy we determined is $E_2=3.76$ for the second atomic layer, while for the first we have $E_1=3.15$ at low temperatures ($T<0.5$) and $E_1'=0.63$ in the high-temperature range ($T>0.5$).

To promote a (110) surface atom from a kink site to the vapor phase, an energy (sublimation energy) $L_0=6\varphi$ is required, where φ is the bond energy in a nearest-neighbor interaction model. An adatom-vacancy pair creation on this perfect surface requires an energy $E_s=7\varphi-5\varphi=L_0/3$, the coordination numbers of a surface atom and an adatom being equal to 7 and 5, respectively.

The value $E_1=3.15$ is in good agreement with the value $E_s=L_0/3=2.6$, where L_0 is the experimental sublimation energy for argon.[25]

The very low apparent activation energy for defect creation in the first atomic layer at high temperatures indicates that the creation process becomes nearly athermal. The high concentration of point defects can explain such a behavior: The probability of creating new defects at the vicinity of preexisting vacancies increases when their concentration increases, thus decreasing the number of broken bonds and the associated apparent activation energy. This mechanism is the one invoked by Burton *et al.*[26] to justify the possible onset of a surface-roughening transition.

The saturation we observed for the defect concentration in the first layer (Fig. 7) implies that the structure of the surface changes when temperature increases and can be taken as a first qualitative indication of a surface roughening.

A phenomenological interpretation of our defect-concentration data using the methods developed by Burton *et al.* has been given recently by Pontikis and Rosato.[27]

B. Order parameter

The high-temperature structure of atomic planes parallel to the surface may be characterized by computing the local order parameter:

$$o_{kl}=(V_1/N_1)\langle\rho_{kl}\rangle=(1/N_1)\left\langle\sum_{j\in l}\exp(i\bar{k}\cdot\bar{r}_j)\right\rangle, \qquad (1)$$

where $j\in l$ means that particle j belongs to the layer l, $\bar{k}$ is the smallest vector of the two-dimensional reciprocal lattice corresponding to a (110) atomic plane $\bar{k}=(0,2\pi/a,0)$, a is the lattice parameter, N is the number of particles contained in layer l at $T=0$ K, and V is the volume of the considered layer.

Choosing a lattice site as the origin of the reference system, we obtain for a perfect layer $o_{kl}=1$, while for a completely disordered one $o_{kl}=0$. This order parameter computed at the surface, say o_{ks}, adequately characterizes the surface structure and thus its possible melting.

Figure 8 shows the results obtained for o_{kl} as a function of layer number at two temperatures. One can see that for surface layers the value decreases more rapidly than for bulk layers.

In Fig. 9 the values of o_{ks} as a function of temperature are shown. The open square is obtained from the MD data of Allen *et al.*,[28] using the following approximate expression for the order parameter:

$$o_{ks}\sim 1-k_y^2\langle u_y^2\rangle/2 . \qquad (2)$$

Equation (2) is easily obtained in the following way: Let us write

$$y_i=y_{i0}+u_{iy} , \qquad (3)$$

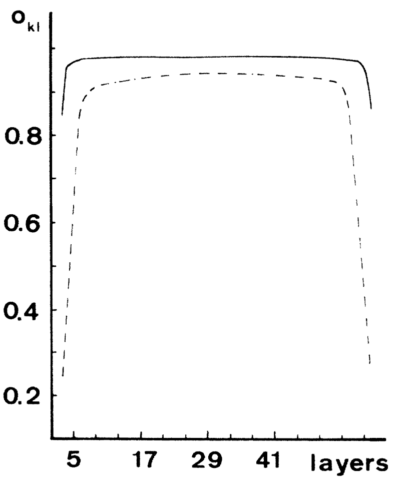

FIG. 8. Local order parameter versus layer number along the normal to free surfaces, $N=2688$. (a) Solid line, $T=0.358$; (b) Dotted-dashed line, $T=0.643$.

TABLE III. Results of the local analysis at thermodynamical equilibrium. N is the total number of particles, N_p the number of (110) planes parallel to free surfaces, T the temperature, and a the experimental lattice parameter we used (in angstroms). L is the number identifying each layer: $L=1$, vapor phase; $L=2$, adatom layer; $L=3$, the first surface layer, etc. $L=B$ corresponds to an atomic layer representative of the bulk. ρ, E, U, P, o_{ks}, and C_v are, respectively, the values of density, total energy, potential energy, pressure, order parameter, and vacancy concentration calculated on a layer basis. The reported values are averaged over equivalent atomic layers of the two free surfaces. For bulk layers the values reported represent an average over ten atomic bulk layers.

N	N_p	T	a	L	ρ	E	U	P	o_{ks}	C_v
673	14	0.330	5.3469	2	0.018	−2.845	−3.340	−0.028	0.009	
				3	0.969	−4.108	−4.603	−0.973	0.917	7.11×10^{-3}
				4	0.990	−6.163	−6.658	0.281	0.972	4.23×10^{-4}
				5	1.020	−7.072	−7.567	−0.001	0.980	0.0
				6	1.025	−7.343	−7.838	−0.153	0.983	0.0
				B	1.030	−7.498	−7.993	−0.332	0.984	0.0
		0.465	5.3901	2	0.144	−2.355	−3.053	−0.159	0.092	
				3	0.800	−3.699	−4.396	−0.754	0.687	1.30×10^{-1}
				4	0.925	−5.456	−6.153	0.103	0.906	1.42×10^{-2}
				5	0.983	−6.410	−7.107	0.106	0.958	1.18×10^{-3}
				6	0.996	−6.984	−7.681	−0.071	0.969	1.15×10^{-4}
				B	1.008	−7.022	−7.179	−0.317	0.974	0.0
		0.583	5.4340	2	0.263	−2.123	−2.997	−0.275	0.102	
				3	0.680	−3.308	−4.182	−0.548	0.428	2.51×10^{-1}
				4	0.862	−4.733	−5.607	−0.144	0.703	5.20×10^{-2}
				5	0.923	−5.666	−6.540	0.119	0.866	8.36×10^{-3}
				6	0.952	−6.151	−7.025	0.016	0.922	4.49×10^{-3}
				B	0.984	−6.526	−7.400	−0.221	0.950	0.0
1345	28	0.617	5.4577	2	0.325	−2.135	−3.060		0.092	
				3	0.684	−3.300	−4.225		0.292	2.73×10^{-1}
				4	0.835	−4.486	−5.411		0.512	9.87×10^{-2}
				5	0.884	−5.311	−6.236		0.708	2.65×10^{-2}
				6	0.916	−5.603	−6.528		0.839	1.54×10^{-2}
				B	0.964	−6.486	−7.411		0.953	0.0
2688	56	0.358	5.3486	2	0.031	−2.770	−3.307	−0.055	0.009	
				3	0.931	−4.000	−4.537	−0.887	0.876	2.85×10^{-2}
				4	0.974	−6.035	−6.572	0.334	0.957	2.19×10^{-3}
				5	1.015	−6.962	−7.499	0.099	0.969	6.4×10^{-4}
				6	1.022	−7.253	−7.790	−0.049	0.973	2.18×10^{-4}
				B	1.031	−7.482	−8.019	−0.403	0.979	0.0
		0.556	5.4342	2	0.320	−2.396	−3.230		0.104	
				3	0.715	−3.593	−4.427	−0.599	0.433	2.46×10^{-1}
				4	0.867	−4.956	−5.790	−0.149	0.686	8.62×10^{-2}
				5	0.932	−5.829	−6.663	0.018	0.837	2.79×10^{-2}
				6	0.963	−6.283	−7.117	−0.044	0.903	6.84×10^{-3}
				B	0.988	−6.745	−7.579	−0.443	0.964	0.0
		0.614	5.4507	2	0.312	−2.161	−3.082		0.114	
				3	0.683	−3.292	−4.213	−0.602	0.294	2.83×10^{-1}
				4	0.843	−4.523	−5.444	−0.345	0.512	1.14×10^{-1}
				5	0.922	−5.398	−6.319	−0.156	0.704	2.74×10^{-2}
				6	0.944	−5.914	−6.835	−0.079	0.846	5.99×10^{-3}
				B	0.975	−6.504	−7.425	−0.345	0.952	0.0
		0.643	5.4621	2	0.398	−2.254	−3.218		0.076	
				3	0.700	−3.336	−4.300	−0.598	0.266	2.81×10^{-1}
				4	0.805	−4.441	−5.405	−0.291	0.456	1.64×10^{-1}
				5	0.880	−5.203	−6.167	−0.043	0.659	5.60×10^{-2}
				6	0.920	−5.675	−6.639	0.049	0.807	1.66×10^{-2}
				B	0.969	−6.364	−7.328	−0.274	0.943	0.0

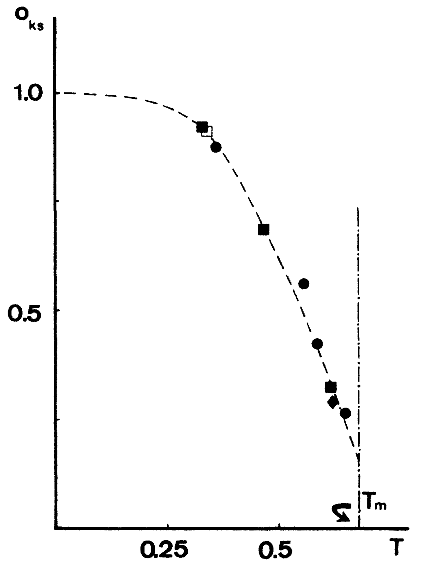

FIG. 9. Temperature dependence of the order parameter for the first atomic layer of our models. Solid circles, $N=2688$; solid squares, $N=673$; solid diamond, $N=1345$; open square, data from Ref. 28. The dashed line is just a guide to the eye.

where y_{i0} and u_{iy} are, respectively, the y components of the equilibrium lattice position and the relative displacement around it of atom i. Introducing Eq. (3) into Eq. (1) and developing to second order in u_{iy}, one obtains Eq. (2) with

$$\langle u_y^2\rangle = (1/N_s)\left\langle \sum_i u_{iy}^2 \right\rangle . \tag{4}$$

Note that in the harmonic approximation, $\langle u_y^2\rangle \sim T$. From Fig. 9 one can see that the value given by Allen *et al.* is in fairly good agreement with those obtained in present study.

The values of o_{ks} remain positive up to a temperature $T=0.643$ very close to the melting point $T_m=0.68$. Therefore they do not support the hypothesis of a liquid-like structure of the surface layers below T_m. However, the steep decay of the order parameter, although inadequate to describe properly the roughening transition, seems to be consistent with its existence. To confirm this point let us analyze the different processes explaining the decay of o_{ks}:

(i) The vacancy concentration at the surface, C_{vs}, reduces the order parameter by a multiplicative factor: $1-C_{vs}$. To correct for this effect we define a new order parameter,

$$o'_{ks} = o_{ks}/(1-C_{vs}) = (1/N'_s)\left\langle \sum_{i\in S} \exp(ik_y y_i)\right\rangle , \tag{5}$$

where N'_s is the mean number of particles belonging to the surface.

(ii) Intralayer diffusion will also reduce the order parameter. The importance of this effect can be roughly estimated by calculating o'_{ks} only over the portions of the atomic trajectories corresponding to a nondiffusive motion. Let us call this overall quantity O^{τ}_{ks}. This leads to

$$O^{\tau}_{ks} \sim o_{ks}(\tau+\tau')/\tau , \tag{6}$$

where τ and τ' are, respectively, the mean residence time and the mean jump duration. To evaluate τ we used the results of De Lorenzi *et al.*[29] These authors showed that the exchange mechanism dominates diffusion on (110) surfaces at low temperatures. Assuming this persists up to the melting point, we evaluated τ at each temperature by extrapolating their results. They are, in reduced units, $\tau_1=22.2$ and $\tau_2=71.43$, respectively, at temperatures $T_1=0.28$ and $T_2=0.24$.

The value of τ' is estimated through

$$\tau' = b/\langle v^2\rangle , \tag{7}$$

where b is the mean jump length and $\langle v^2\rangle$ the mean-square velocity at the given temperature.

Correcting the order parameter for these two effects, one obtains a value which includes only the effect of thermal motion of atoms around their equilibrium sites.

In Fig. 10, O^{τ}_{ks} is plotted as a function of temperature, and we compare it with the linear extrapolation of the order parameter from the low-temperature range, where diffusion and defect concentration are negligible.

The temperature corresponding to the departure of O^{τ}_{ks} values from the extrapolation of the low-temperature data can be used to define the roughening transition temperature. The value we obtain, $T=0.55$, is consistent with that deduced from the vacancy-concentration data given in Fig. 7, $T\sim 0.5$. The validity of our conclusions depends on whether or not our systems really reached the

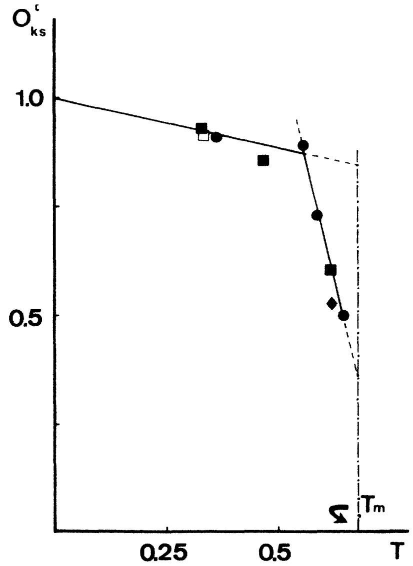

FIG. 10. Temperature dependence of the order parameter O^{τ}_{ks} and comparison with the extrapolation of its low-temperature behavior up to the melting point. Solid circles, $N=2688$, solid diamond, $N=1344$; solid squares, $N=673$; open square, data from Ref. 28.

thermodynamic equilibrium. This has been checked by investigating the phase diagram, but this procedure cannot identify a possible metastability of the surface-layer structure. More specifically, one can ask if the surface roughening we observed is just the dynamical process of surface melting possibly not completed during our MD runs. A strong indication against this possibility and supporting our main conclusions is given by the following argument:

In our systems surface melting can occur through the collective motion of surface atoms, which was interpreted in our analysis as the spontaneous creation of point-defect pairs. Close to the bulk melting point, the activation energy $E_1' = 0.63$ we determined for this process gives an order of magnitude of the associated characteristic time by using the expression

$$\tau_c = \tau_0 \exp(-0.63/T) , \tag{8}$$

where $\tau_0 = 1/\nu_{\max}$, and $\nu_{\max}$ is the maximum vibrational frequency of the solid. Taking $\nu_{\max} \sim 2$ Thz,[28] $T = 0.643$, one obtains $\tau_c \sim 1.33$ ps, corresponding to a trajectory length of 133 time steps. We therefore argue that the surface melting can easily take place during the equilibration trajectories (4000 time steps) and the equilibrium ones (4100 time steps), but this was not observed even at the highest temperature we investigated.

In a recent paper Gorse *et al.*[30] reported experimental results obtained by helium atomic-beam diffraction on (110) copper surfaces. They observed a dramatic decrease of the diffracted intensity by increasing temperature, similar to that previously observed for copper vicinals.[14] This is interpreted as the onset of a high disorder on the surface. Their results are consistent with the onset of a roughening transition on the (110) surface, and are very similar to those obtained in present study.

C. Self-diffusion

The detailed study of the surface self-diffusion confirmed the results of previous MD studies[29,31] and the suggestions of recent experimental work.[32] According to them the diffusion process on (110) fcc surfaces is dominated by the exchange mechanism in the low- and intermediate-temperature range. It allows for parallel or cross-channel migration of the adatoms. Figures 11(a)–11(c) illustrate this mechanism for a cross-channel adatom jump. Figure 11(b) shows the saddle-point atomic configuration.

In the high-temperature range and for $N = 2688$ the atomic surface self-diffusion coefficient has been calculated using the Kubo formulas. An activation energy $E_D = 5.58$ was obtained. Due to the surface roughening and to the various delocalized jumps which contribute considerably to diffusion at these temperatures,[12,29] the respective contributions to E_D, resulting from the formation and the migration energies of the defects, cannot be simply resolved.

As mentioned in the Introduction, the high surface diffusivities observed experimentally have been sometimes attributed to the possible melting of surface layers just because their values were comparable to those obtained for the bulk liquid. In order to test such a qualitative argument, we report in Fig. 12 the Arrhenius plots of our results together with diffusion data obtained for (i) liquid argon [experimental (Ref. 33)], (ii) the surface of a supercooled liquid (MD, Ref. 34), (iii) the bulk supercooled liquid [MD, Ref. 6(a)], and (iv) the (110) argon surface [MD, Refs. 6(c) and 31]. One can see from this figure that our results (solid circles) are in good agreement with those obtained by Broughton and Gilmer[6(c)] (solid diamonds rhombs) and by Mruzik and Pound[31] (solid triangles). The surface diffusivities reach values comparable with those of a supercooled liquid surface only near the melting point.

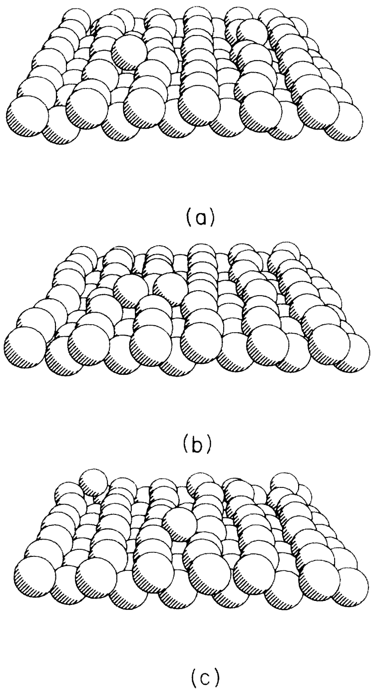

FIG. 11. Snapshots illustrating the exchange mechanism for adatom migration on (110) surfaces. (a) and (c), adatom in the equilibrium sites; (b), saddle-point position.

In the high-temperature range they are greater than the diffusivity values for the bulk supercooled liquid and the ones corresponding to liquid argon at the triple point. Moreover, diffusion is an athermal process in liquids but is thermally activated for the MD data of the (110) surface presented in Fig. 12, as indicated by the slope of the line fitting our results. This behavior confirms that surface layers are not melted, but are highly disordered at high temperatures.

To conclude let us emphasize that an overly simplistic comparison of surface and liquid diffusivities can lead to wrong conclusions concerning the structure of surfaces.

IV. CONCLUSION

In the present paper we have studied the temperature dependence of the structure of a (110) surface of solid ar-

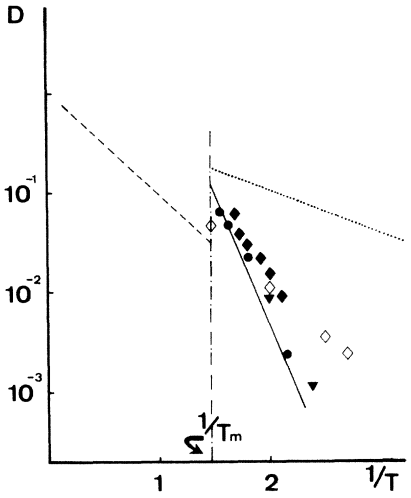

FIG. 12. Arrhenius plots of diffusion coefficients. (a) (110) surface; solid circles, this study, $N=2688$ data for the first atomic layer; solid diamonds, data from Ref. 6(c); solid triangles, data from Ref. 31. (b) Dotted line, surface diffusivity for a supercooled liquid from Ref. 34. (c) Dashed line, extrapolation at $p=0$ from the experimental diffusion data for the bulk liquid, from Ref. 33. (d) Open diamonds, diffusion data for a supercooled liquid from Ref. 6(a).

gon. We have found that the stability of the MD model strongly depends on the surface-to-volume energy ratio. Therefore small models with large surfaces are unreliable because the melting of these systems occurs at temperatures lower than the thermodynamical melting point. We used a model large enough to avoid such an instability.

Upon increasing the temperature, the surface undergoes a structural transition which can be qualitatively identified with a roughening transition. This conclusion is supported by the saturation of the defect concentration and the decay of the order parameter in the high-temperature range $T>0.7T_m$.

In spite of the roughening, we find no evidence of surface melting up to the melting point. In fact, the order parameter retains a high nonzero value up to T_m. This supports the point of view that the structure of the surface is greatly disordered but still crystalline.

The results obtained for self-diffusion coefficients are in agreement with the given picture of the surface structure. They are close to the diffusion coefficient of a supercooled liquid surface, but only the diffusion on a crystalline surface is an activated process.

ACKNOWLEDGMENTS

It is a pleasure to thank Y. Adda, C. Moser, M. Guillope, M. Meyer, M. Parrinello, and E. Tosatti for stimulating discussions. Generous allocation of computer time from Istituto Nazionale di Fisica Nucleare (sezione di Roma) is gratefully acknowledged. We are grateful to M.Gillan and I. McDonald for the critical reading of the manuscript. One of us (V.P.) acknowledges D. Gorse and J. Lapujoulade for kindly providing copies of their recent works prior to publication; another of us (V.R.) acknowledges financial support from EURATOM through Grant No. JD/hp-XII/355/82-IT, and another (G.C.) financial support from Centre Européen de Calcul Atomique et Moléculaire (CECAM), Orsay and Section de Recherches de Métallurgie Physique (SRMP).

APPENDIX

Potential energy and pressure should be corrected to include the long-range contributions (LRC's). These corrections are not the "standard" ones due to the existence of free surfaces in our model and are evaluated by as following:

$$U_{\rm LRC}=\tfrac{1}{2}\rho\int_D g(r)V(r)d^3r\,, \qquad \text{(A1)}$$

$$P_{\rm LRC}=-\tfrac{1}{6}\rho^2\int_D g(r)r\frac{dV(r)}{dr}d^3r\,, \qquad \text{(A2)}$$

where ρ is the density, $g(r)$ the radial distribution function, $V(r)$ the potential, and D the domain of integration.

For our systems the domain D is the complement to the spherical domain displayed in Fig. 13. The last is defined by a sphere, the radius of which is equal to the potential cutoff radius and, eventually, its intersections with the free surface depending on the location of the considered layer.

Thus, for energy, Eq. (A1) becomes

$$U_{\rm LRC}=\pi\rho\left[\int_{\pi/2}^{\pi}\sin\theta\,d\theta\int_{r_c}^{R_2}V(r)r^2dr + \int_{\theta_0}^{\pi/2}\sin\theta\,d\theta\int_{r_c}^{R_1}V(r)r^2dr\right], \qquad \text{(A3)}$$

where

$$R_1=\frac{d_1}{\cos\theta},\quad R_2=\frac{d_2}{\cos\theta},\quad \cos\theta_0=\frac{d_1}{r_c}\;;$$

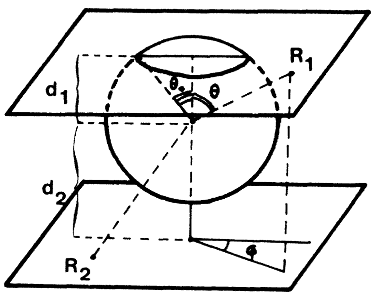

FIG. 13. Scheme illustrating the domain over which the long-range correction for energy and pressure is calculated for our models.

we set $g(r)=1$ for $r>r_c$ and $V(r)\cong -4\epsilon(\sigma/r)^6$. A similar equation is obtained for pressure.

The final result for energy and pressure, respectively, for a layer l lying at distances d_1 and d_2 from the free surfaces are

$$U_{\text{LRC}}=\begin{cases} -\dfrac{\pi\rho d_1}{r_c^4}+\dfrac{4\pi\rho}{3}\left[\dfrac{1}{4d_2^3}-\dfrac{1}{r_c^3}\right], & d_1<r_c,\ d_2>r_c \\[2ex] -\dfrac{4\pi\rho}{3}\left[\dfrac{1}{4}\left[\dfrac{1}{d_1^3}+\dfrac{1}{d_2^3}\right]-\dfrac{2}{r_c^3}\right], & d_1>r_c, d_2>r_c \end{cases} \tag{A4}$$

$$P_{\text{LRC}}=\begin{cases} -\dfrac{2\pi\rho^2 d_1}{r_c^4}+\dfrac{8\pi}{3}\rho^2\left[\dfrac{1}{4d_2^3}-\dfrac{1}{r_c^3}\right], & d_1<r_c, d_2>r_c \\[2ex] \dfrac{8\pi}{3}\rho^2\left[\dfrac{1}{4}\left[\dfrac{1}{d_1^3}+\dfrac{1}{d_2^3}\right]-\dfrac{2}{r_c^3}\right], & d_1>r_c,\ d_2>r_c. \end{cases} \tag{A5}$$

The case $d_1<r_c$ and $d_2<r_c$ is not considered, because even for the smallest system we studied, the thickness of the model, L, is such that $L=d_1+d_2>2r_c$.

---

*To whom correspondence should be addressed.

[1] J. K. Kristensen and R. M. J. Cotterill, Philos. Mag. **36**, 437 (1977).

[2] L Pietronero and E. Tosatti, Solid State Commun. **32**, 255 (1979).

[3] C. S. Jayanthi, E. Tosatti, and A. Fasolino, Phys. Rev. B **31**, 470 (1985).

[4] C. S. Jayanthi, E. Tosatti, and L. Pietronero, Phys. Rev. B **31**, 3456 (1985).

[5] J. Q. Broughton and L. V. Woodcock, J. Phys. C **11**, 2743 (1979).

[6] (a) J. Q. Broughton and G. H. Gilmer, J. Chem. Phys. **79**, 5095 (1983); (b) **79**, 5105 (1983); (c) **79**, 5119 (1983).

[7] G. H. Gilmer and J. Q. Broughton, J. Vac. Sci. Technol. B **1**, 298 (1983).

[8] *Course of Statistical Thermodynamics*, edited by L. D. Landau and E. M. Lifshitz (Mir, Moscow, 1965).

[9] N. A. Gjostein, in *Surfaces and Interfaces I. Chemical and Physical Characteristics*, edited by J. J. Burke, N. L. Reed, and N. V. Weiss (Syracuse University Press, Syracuse, NY, 1967), p. 271.

[10] H. P. Bonzel, in *Surface Physics of Materials*, edited by J. M. Blakely (Academic, New York, 1975), p. 279.

[11] (a) G. E. Rhead, Surf. Sci. **15**, 353 (1969); (b) **22**, 223 (1970).

[12] N. A. Gjostein and H. P. Bonzel, Surf. Sci. **22**, 216 (1970).

[13] (a) G. Fritsch, R. Lachner, H. Diletti, and E. Luscher, Philos. Mag. **46**, 829 (1982); (b) **50**, 545 (1984).

[14] J. Lapujoulade, J. Perreau, and Kara, Surf. Sci. **129**, 59 (1983).

[15] J. Villain, D. Grempel, and J. Lapujoulade, J. Phys. F **15**, 809 (1985).

[16] R. Kikuchi and J. W. Cahn, Phys. Rev. B **21**, 1893 (1980).

[17] G. Ciccotti, M. Guillope, and V. Pontikis, Phys. Rev. B **27**, 5576 (1983).

[18] R. M. Goodman and J. A. Somorjai, J. Chem. Phys. **52**, 6325 (1970).

[19] C. L. Briant and J. L. Burton, J. Chem. Phys. **63**, 2045 (1975).

[20] L. Verlet, Phys. Rev. **159**, 98 (1967) (the time unit used in this paper is smaller than ours by a factor of $\sqrt{48}$).

[21] G. L. Pollack, Rev. Mod. Phys. **36**, 748 (1964).

[22] R. P. Gupta, Phys. Rev. B **23**, 6265 (1981).

[23] *Gas Encyclopedia* (Division Scientifique de l'Air Liquide/Elsevier, Amsterdam, 1976).

[24] J. P. Hansen and M. K. Klein, Phys. Rev. B **13**, 878 (1976).

[25] G. K. Horton, Am. J. Phys. **36**, 93 (1968).

[26] W. K. Burton, N. Cabrera and F. C. Frank, Philos Trans. R. Soc. London, Ser. A **243**, 299 (1951).

[27] V. Pontikis and V. Rosato, in Proceedings of the 7th European Conference on Surface Science, ECOSS-7, 1–4 April 1985, Aix-en-Provence, France [Surf. Sci. (to be published)].

[28] R. E. Allen, F. W. de Wette, and A. Rahman, Phys. Rev. **179**, 887 (1969).

[29] G. de Lorenzi, G. Jacucci, and V. Pontikis, Surf. Sci. **116**, 391 (1982).

[30] D. Gorse and J. Lapujoulade, in Ref. 27.

[31] M. R. Mruzik and G. M. Pound, J. Phys. F **11**, 1403 (1981).

[32] D. Ghaleb and B. Peraillon, in Ref. 27.

[33] J. Naghizadeh and S. A. Rice, J. Chem. Phys. **36**, 2710 (1962).

[34] M. R. Mruzik, S. H. Garofalini, and G. M. Pound, Surf. Sci. **103**, 353 (1981).